The Basis for k^*_{cat} Impairment in Prophospholipase A_2 from the Anion-Assisted Dimer Structure[†,‡]

Todd M. Epstein, Bao-Zhu Yu, Ying H. Pan, Stephen P. Tutton, Badri P. Maliwal,[§] Mahendra K. Jain, and Brian J. Bahnson*

Department of Chemistry and Biochemistry, University of Delaware, Newark, Delaware 19716

Received June 14, 2001; Revised Manuscript Received July 30, 2001

ABSTRACT: Kinetic results in this paper show that, contrary to earlier reports, pig pancreatic prophospholipase A_2 (proPLA2) does not hydrolyze monodisperse short chain phosphatidylcholine below the critical micelle concentration. ProPLA2 is active on an anionic interface, but at a rate that is decreased by more than 100-fold compared to that of PLA2, the active form. Solution studies show that both proPLA2 and PLA2 bind to an anionic interface and also bind a tetrahedral intermediate mimic at the active site. The 1.5 Å resolution crystal structure of the anion-assisted dimer of proPLA2 reported in this paper is compared with the corresponding structure for PLA2 [Pan, Y. H., et al. (2001) *Biochemistry 40,* 609−617]. As a mimic for the forms bound to the anionic interface, these structures provide insights into the possible structural basis for the impaired chemical step of the zymogen. The proPLA2 dimer contained within one crystallographic asymmetric unit has one molecule of the inhibitor 1-hexadecyl-3-(trifluoroethyl)-*sn*-glycero-2-phosphomethanol and is bridged by four coplanar sulfate anions. Relative to the structure of PLA2, the subunit contact surface in proPLA2 displays a tilted orientation, an altered mode of inhibitor binding, displacement of a mechanistically significant loop that includes Tyr69, and a critical active site water seen in PLA2 that is not seen in proPLA2. These differences are interpreted to suggest possible origins of the functional differences between the pro and active enzyme at an anionic interface. A structural origin of this difference is discussed in terms of the calcium-coordinated activated water mechanism of the esterolysis reaction. Together, a comparison of the structures of the anion-assisted dimers of PLA2 and proPLA2 not only offers an explanation of why the zymogen form is k^*_{cat}-impaired and binds poorly even to the anionic interface but also supports a mechanism for the activated enzyme that includes a critical second-sphere assisting water bridging His48 and the calcium-coordinated catalytic water.

Phospholipase A_2 (PLA2)[1] catalyzes the hydrolysis of the *sn*-2 acyl chain of aggregated phospholipids through the interfacial processive turnover mechanism shown in Scheme 1 (*1*, *2*). The crystal structures of PLA2 (*3*−*5*) coupled with kinetic and biochemical studies have led to consensus models that begin to describe the regulation and specificity of interfacial catalysis (*6*, *7*). The pancreatic PLA2 is secreted in a zymogen form (proPLA2) with a seven-residue prosequence at the N-terminus, which is cleaved to become functionally active. Compared to PLA2, proPLA2 has a greatly reduced activity at an interface (*8*, *9*), which raises questions about the contributions of the various structural features needed for the catalytic activity of PLA2 at an interface. In the context of Scheme 1, such differences could result from a difference in the events of the turnover cycle, the binding of the enzyme to the interface, or the underlying allosteric changes induced by the interface.

Scheme 1

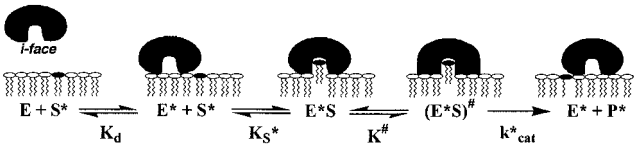

In this paper, we evaluate the differences between the kinetic and interfacial properties of proPLA2 and PLA2 in terms of their structures. In addition to some of the critical unresolved issues about the kinetic behavior of proPLA2, the previously reported structures of proPLA2 (*10*−*12*) have not provided the necessary basis for the functional differences relative to PLA2. In these structures, the N-terminus of proPLA2 is disordered and the active site did not have a substrate mimic or ligand bound. These structures were interpreted to suggest that the propeptide impairs function

[†] The research was supported by NIH Grant GM-29703 (M.K.J. and B.J.B.) and NIH Training Grant T32 GM-08550 (T.M.E.).

[‡] Coordinates for the structure of prophospholipase A_2 have been deposited in the Protein Data Bank as entry 1HN4.

* To whom correspondence should be addressed. Telephone: (302) 831-0786. Fax: (302) 831-6335. E-mail: bahnson@udel.edu.

[§] Current address: Department of Biological Chemistry, University of Maryland Medical School, Baltimore, MD 21201.

[1] Abbreviations: *B*-factor, temperature factor; calcium-binding loop, residues 26−34 of PLA2 that provide backbone carbonyl oxygens from positions 28, 30, and 32 as ligands to bound calcium; CMC, critical micelle concentration; DC_nPC, 1,2-diacyl-*sn*-glycero-3-phosphocholine with *n* carbons in each acyl chain; DC_nPM, 1,2-diacyl-*sn*-glycero-3-phosphomethanol with *n* carbons in each acyl chain; DC_8PM-ether, 1,2-dioctyl-*sn*-glycero-3-phosphomethanol; deoxy-LPC, 1-hexadecyl-propanediol-3-phosphocholine; HDS, hexadecyl sulfate; i-face, interface binding surface of the enzyme; MJ33, 1-hexadecyl-3-(trifluoroethyl)-*sn*-glycero-2-phosphomethanol; PDB, Protein Data Bank; PLA2, phospholipase A_2; proPLA2, prophospholipase A_2; rmsd, root-mean-square deviation; R_{free}, free *R*-factor; $R_{working}$, working *R*-factor; $X_I(50)$, inhibitor mole fraction of half-activity; 69-loop, residues 61−72 of PLA2, including Tyr69.

10.1021/bi011228h CCC: $20.00
Published on Web 08/29/2001

by the disruption of a critical hydrogen bond network that includes the N-terminus of the enzyme (*3*). Not only is the role of this network in the catalytic cycle questionable (*13*, *14*), the previously determined structures of proPLA2 do not necessarily represent the structural form of the enzyme bound to the substrate interface. This raises the point that it is critical to obtain structural insights into interfacial enzymes in a form that mimics their interaction with an interface.

In this paper, we show that proPLA2 is k^*_{cat}-impaired at the anionic interface. Although PLA2 is 100-fold more active than proPLA2 at the anionic interface, both forms of the enzyme are totally inactive with monodisperse short chain zwitterionic phosphatidylcholines below their CMC. Independent measurements in solution with suitable interfaces show that proPLA2 binds to anionic interfaces, and the bound form also binds the competitive inhibitor 1-hexadecyl-3-(trifluoroethyl)-*sn*-glycero-2-phosphomethanol (MJ33) and calcium in the active site. On the basis of leads from these functional studies and previous structural work on the anion-assisted dimer of PLA2 (*15*), the anion-assisted dimer of proPLA2 was crystallized in a form that mimics its interaction with an anionic interface. We present the structure of the dimer of proPLA2 complexed with one molecule of MJ33 and four coplanar sulfate anions to a resolution of 1.5 Å. Compared to PLA2 (*15*), the contact surface of the proPLA2 dimer and the orientation of MJ33 in the active site are different. Furthermore, the relationship of anion binding sites, the dimer contact surface, and the subunit bridging nature of the inhibitor strongly suggest that the dimer interface is representative of the putative interface binding surface (i-face) of proPLA2 (*16*) involved in the binding to an anionic interface. A comparison of the structural features of the anion-assisted dimeric forms of proPLA2 and PLA2 shows subtle differences in the orientation of the tetrahedral intermediate mimic. The notable absence of a mechanistically critical water molecule in the proPLA2 structure, which is found in the PLA2 structure, suggests an explanation for the k^*_{cat} impairment.

EXPERIMENTAL PROCEDURES

Kinetics for ProPLA2 versus PLA2. Sources of enzymes, reagents, and experimental protocols were the same as those described previously (*17*−*19*). Unless indicated otherwise, all measurements were taken in 1 mM $CaCl_2$ and 10 mM Tris at pH 8.0 and 24 °C. Other specific conditions are given below. The observed rate of hydrolysis of diacylglycero-phospholipid substrates was measured in parallel for proPLA2 and PLA2 using materials and conditions described previously (*14*, *20*). The rate of hydrolysis was measured for zwitterionic substrates 1,2-diacylglycero-*sn*-3-phosphocholine with 6 or 7 (*n*) carbons in each acyl chain (DC_nPC) and also with anionic substrates 1,2-diacylglycero-*sn*-3-phosphomethanol with 8 or 14 (*n*) carbons in each acyl chain (DC_nPM). The kinetics of proton release by PLA2-catalyzed hydrolysis were measured by the pH-stat method (*1*, *2*) using a Brinkman (Metrohm) or a Radiometer titrator (PHM290) with a 3 mM NaOH or 2-aminopropanediol (AMPD) titrant in the buret in the presence of 1 mM $CaCl_2$.

Measurement of the change in the absorbance spectrum and related measurements were carried out on an HP8452 UV−vis diode array spectrophotometer. The uncorrected MJ33-induced change in the UV absorption spectrum was measured with a solution of 0.035 mM porcine proPLA2 or PLA2 in the presence of 3 mM 1-hexadecylpropanediol-3-phosphocholine (deoxy-LPC) at pH 8.0 in 10 mM Tris-HCl (*21*).

Fluorescence Emission Spectroscopy. Binding of porcine pancreatic proPLA2 and PLA_2 (∼1 μM) to 1,2-dioctylphosphatidylmethanol (DC_8PM-ether) was monitored as the change in fluorescence at 333 nm (excitation at 280 nm) on an SLM-Aminco AB2 luminescence spectrometer with magnetic stirring in a cuvette containing 1.5 mL of 100 mM NaCl, 1 mM $CaCl_2$, and 10 mM Tris (pH 8.0). These experiments were performed with PLA2 and proPLA2 at closely matched concentrations, therefore eliminating the need for normalization of the intensity scale. Typically, the slit widths were kept at 4 nm each, and the sensitivity (PMT voltage) was adjusted to 1% for the Raman peak corresponding to the same excitation wavelength from the buffer blank. The relative change in fluorescence (δF) is defined as $(F - F_0)/F_0$, where F_0 and F are the intensity without and with phospholipid, respectively.

Dissociation Constants for ProPLA2 and PLA2 Complexes. Detailed experimental protocols for the determination of equilibrium dissociation constants for inhibitors bound to E or E* have been described (*19*). Equilibrium dissociation constants for an inhibitor (K_I*) or calcium (K_{Ca}*) for PLA2 were determined by the protection method (*17*) in 1 mM NaCl at pH 7.4 in cacodylate buffer. Values of the interfacial equilibrium parameters are expressed in mole fraction units, and the estimated uncertainty in the dissociation constant values is less than 30%. The protection method could not be adopted for proPLA2; however, as described in this paper, the change in the UV absorbance induced by MJ33 is a useful measure of the occupancy of the active site.

Measurement of Aggregate Particle Size. These procedures are described thoroughly elsewhere (*22*). Light-scattering measurements for generating Zimm or Debye plots were carried out with the help of K. Koehler in his laboratory at Case Western Reserve University (Cleveland, OH) on a model B variable multiangle light-scattering instrument from Wyatt Technology Corp. (Santa Barbara, CA) equipped with a DAWN data processing system. Typically, these results were obtained at 3−50 μM PLA2 alone, or with 0.1−15 μM PLA2 with 5−200 μM DC_8PM-ether in 0.5 mM $CaCl_2$ and 10 mM Tris at pH 8.0. Dynamic light-scattering measurements were taken on a SynaPro 801 instrument from Protein Solutions through the courtesy of F. Lewandowski, who also carried out data analysis with the software available with the instrument. Uncertainty in the particle size obtained by this method is typically less than 15%. Concentrations of PLA2 from 0.3 to 1 mM are required for the determination of the particle size in the absence of phospholipids. On the other hand, due to formation of large particles in the presence of phospholipids, typically, 10−15 μM PLA2 was found to be adequate for most measurements with enzyme associated with anionic phospholipids, even under the premicellar conditions.

Crystallization and X-ray Data Collection. Porcine proPLA2 suitable for crystal growth and the competitive inhibitor MJ33 were obtained as previously described (*23*). Crystals of the proPLA2−MJ33 complex were grown at 25 °C from 2 μL hanging drops containing 15 mg/mL proPLA2, 10 mM

$CaCl_2$, 3 mM MJ33, 0.2 M $(NH_4)_2SO_4$, and 0.1 M Na^+-acetate adjusted to pH 4.6. Crystals typically appeared within 2 days and grew to dimensions of 0.3 mm × 0.3 mm × 0.1 mm. Crystals were equilibrated in a cryoprotecting solution made of the reservoir crystallization solution with the addition of xylitol to a concentration that was 35% saturated. Crystals were flash-frozen in liquid nitrogen and kept frozen in a −180 °C nitrogen cryostream during data collection. X-ray diffraction data sets were collected from a single crystal on a Rigaku RU-H3R rotating anode generator, OSMIC confocal optics, and a RAXIS IV image plate area detector. The proPLA2−MJ33 crystal was indexed and processed in space group $P2_1$ using the programs DENZO and SCALEPAK (*24*).

Molecular Replacement and Crystallographic Refinement. The structure of the proPLA2−MJ33 complex was determined via molecular replacement using the program CNS (*25*). The starting model was the porcine PLA2 structure (PDB entry 1P2P) previously reported without water molecules (*26*). The final molecular replacement solution included two subunits of the PLA2 monomer in the asymmetric unit. X-ray structure refinement was performed using the program CNS (*25*). The molecular replacement solution was initially refined by a standard protocol of rigid body refinement, simulated annealing, and positional refinement with a maximum likelihood target using amplitudes. The Ca-binding loop (residues 26−34) of each subunit was significantly different from the original molecular replacement search model and was built into difference electron density maps ($2F_o - F_c$ coefficients). The 69-loop (residues 61−72) of PLA2 was not present in the search model and was likewise built in as phases were improved during the model building and refinement process. The 7-mer propeptide, QEGISSR, was then built from the known porcine PLA2 sequence (Swiss Prot entry P00592). Regions of the structure were corrected during refinement using a composite simulated annealing omit map (*27*). Additionally, protein geometry was analyzed using PROCHECK (*28*) and corrected accordingly. One residue, Ile−4[2] of subunit B, was found in a disallowed region of a Ramachandran plot. The residue is located in a tight turn stabilized by an H-bond interaction between the carboxyl oxygen of Gly−5 and amide nitrogen of Ser−3 and has clearly interpretable electron density. Ordered water molecules were automatically built into difference electron density maps ($F_o - F_c$) using the wat-pick feature of CNS (*27*), and then inspected individually for proper distance and H-bonding interactions. Alternate conformations of several side chains were found past C_β and refined with occupancies of 0.5 for each conformation that was modeled. The final converged model had a free *R*-factor (R_{free}) of 0.239 and a working *R*-factor ($R_{working}$) of 0.215 refined with diffraction data to a resolution of 1.5 Å. Further crystallographic refinement attempted with the program SHELXL-97 (*29*) was unsuccessful at reducing the R_{free} or $R_{working}$.

RESULTS

The catalytic and spectroscopic properties of the zymogen proPLA2 and active form PLA2 are compared under a variety of conditions, including the monodisperse and interface-associated forms. We carried out detailed studies to understand the binding and catalytic function of proPLA2 at zwitterionic and anionic interfaces. Previous reports of activities for monodisperse substrates with proPLA2 (*6*, *8*, *9*, *30*−*32*) are called into question by the observation that PLA2 is catalytically inert on monodisperse phosphatidylcholines, and that the activity observed in stirred solutions is due to the reaction on the vessel walls (*20*). These and other results obtained under conditions relevant for the evaluation of the active site occupancy and the binding to the interface (Scheme 1) are summarized first, and then their significance is evaluated on the basis of the crystallographic structure of proPLA2.

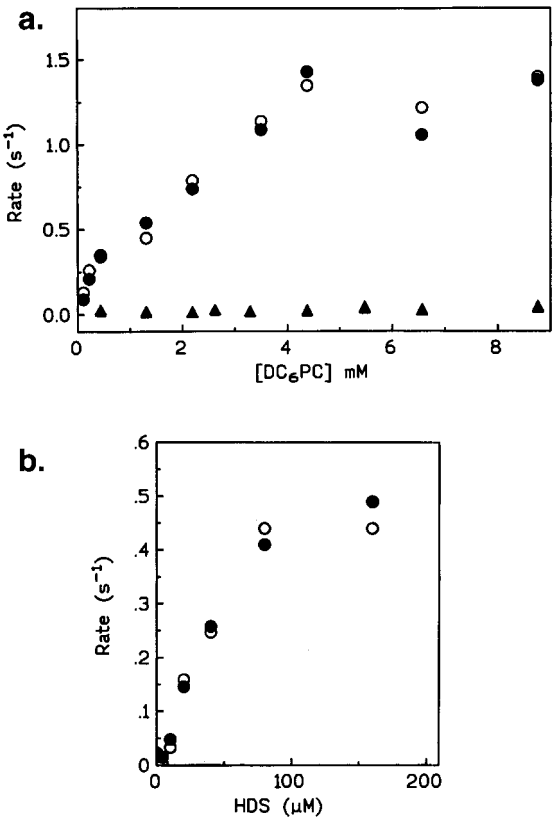

FIGURE 1: (a) Observed rate of hydrolysis of DC_6PC by proPLA2 in a stirred (black symbols) and unstirred (white symbols) reaction mixture containing 1 mM (▲) and 4 M NaCl (● and ○) at 25 °C. The critical micelle concentration for DC_6PC is 16 mM in 1 mM NaCl and 3.5 mM in 4 M NaCl. (b) A 20-fold increase in the rate of hydrolysis of monodisperse DC_6PC is seen in the presence of monodipserse HDS, whose CMC > 0.5 mM.

Several interesting features of the proPLA2-catalyzed rate may be noted. As developed below, four sets of conditions are compared for proPLA2 and PLA2: the hydrolysis of monodisperse or aggregated zwitterionic phosphatidylcholines and the hydrolysis of anionic DC_nPM monomers or their aggregates formed in the presence of the enzymes. Note that it is difficult to characterize the substrate behavior of monodisperse anionic phospholipids because these amphiphiles form premicellar aggregates. Similar aggregates are formed with zwitterionic phosphatidylcholines in the presence of 4 M NaCl. Previously published monomer kinetic results are unreliable because such effects are not adequately dissected.

As shown in Figure 1a, the rate of hydrolysis of the zwitterionic substrate DC_6PC by proPLA2 in 1 mM NaCl is

[2] The negative sign in front of the residue number indicates its propeptide position relative to the active enzyme's N-terminus.

Table 1: Apparent Maximum Rates (s^{-1}) of Hydrolysis of ProPLA2 and PLA2

assay conditions	proPLA2	PLA2
DC6PC monodisperse[a] (1 mM NaCl)	<0.01	<0.02
DC6PC micelles (1 mM NaCl)	0.01	6
DC6PC micelles (4 M NaCl)	1.3	240
DC_7PC monodisperse (1 mM NaCl)	<0.03	<0.03
DC_7PC micelle (1 mM NaCl)	<0.03	16
DC_7PC micelle[a] (4 M NaCl)	4	660
DC_8PM premicellar (1 mM NaCl)	5	1100
DC_{14}PM vesicles (1 mM NaCl)	0.3	300

[a] For the charge-compensated bovine K53,56,120M and K53,56,120,121M mutants of proPLA2 and PLA2, the rate with monodisperse DC_7PC is less than 0.05 s^{-1}. The rates for the mutant PLA2s with micellar DC_7PC with 4 M NaCl are between 5 and 10 s^{-1}, compared to the rates of 400−900 s^{-1} with PLA2 (*36*). The rate of hydrolysis with the charge-compensated proPLA2 mutants was typically <1 s^{-1} at the zwitterionic DC_7PC micelles.

less than 0.01 s^{-1}, compared to the value of 1.3 s^{-1} seen in the presence of 4 M NaCl. On the basis of these and other results in Table 1, we conclude that the rate of hydrolysis of monodisperse short chain phosphatidylcholines is immeasurably small with proPLA2 as well as with PLA2. As a control, the kinetic behavior of purified proPLA2 under the various assay conditions suggests that the amount of PLA2 impurity is less than 0.01%. This estimate is consistent with the purity of the proPLA2 preparation used for these studies, which was freshly purified with baseline separation from PLA2 by anion exchange chromatography. The insignificant rates for monodisperse substrates with proPLA2 in solution (Table 1) suggest that the catalytic rate with proPLA2 reported earlier with premicellar monodisperse zwitterionic substrates (*8*) was an artifact due to activation by salt present in the assay mixture and the reaction on the extraneous surfaces as shown to be the case with PLA2 (*20*).

Both PLA2 and proPLA2 show an enhanced rate of hydrolysis of short chain phosphatidylcholines in 4 M NaCl; however, the rate with proPLA2 is considerably smaller than that seen with PLA2 (Table 1). The fact that virtually the same rate of hydrolysis was observed under the stirred and unstirred conditions in the fluorescence assay (Figure 1a) with the monodisperse substrate shows that the observed rate in 4 M NaCl with either of these enzymes is not due to the reaction on the cuvette surface (*20*). The apparent activating effect of 4 M NaCl is attributed to the anionic charge induced by the partitioning of chloride in the zwitterionic premicellar interface (*33*). Likewise, the 20-fold increase in rate in the presence of hexadecyl sulfate (HDS) with the zwitterionic substrate DC_6PC (Figure 1b) corroborates a role of anionic interface activation. These results show that the activity of proPLA2 on the monodisperse phosphatidylcholine or at the zwitterionic interface is immeasurably small (<0.1 s^{-1}) unless an anionic interface is also present.

Furthermore, a significant rate of proPLA2-catalyzed hydrolysis is also seen with anionic substrates. As summarized in Table 1, anionic monodisperse DC_8PM and vesicles of DC_{14}PM are hydrolyzed by proPLA2 at a measurable rate, yet the process is significantly slower than with PLA2. As also indicated in the footnote of Table 1, the charge-compensated mutants of bovine proPLA2 also exhibit activities comparable to those with the pig pancreatic proPLA2. These results essentially rule out an allosteric effect

Table 2: Dissociation Constants (mM) for ProPLA2 and PLA2 Complexes

dissociation step[a]	proPLA2	PLA2
E−Ca → E + Ca	0.175	0.32
E*−Ca → E* + Ca	0.175	0.25
E*−Ca−MJ33 → E* + Ca + MJ33	0.15	0.005
E*−Ca−MJ33 → E−Ca−MJ33	0.25	0.03
E* → E	>30	3

[a] The nomenclature of E and E* is presented in Scheme 1. Unless otherwise noted, E* refers to the enzyme associated with a deoxy-LPC aggregate (*17*).

where the prosequence directly interacts with residues 53, 56, 120, and 121. Together, results in Table 1 and Figure 1 show that proPLA2 catalyzes the hydrolysis at the anionic interface at a rate that is 0.1−1% of the rate measured with PLA2. Additional results (not shown here) showed that both PLA2- and proPLA2-catalyzed hydrolysis of DC_{14}PM vesicles are inhibited by MJ33 at comparable mole fractions. If K_M* for the substrate DC_{14}PM is comparable for both the enzymes, or if both K_M* for the substrate and K_I* for MJ33 change comparably, a lower rate at the maximum possible mole fraction of the substrate on the interface ($X_S = 1$) implies that proPLA2 is k^*_{cat}-impaired.

Parameters for Binding of ProPLA2 to Preformed Aggregates. Results summarized in Table 2 show that proPLA2 binds to the anionic interface. Although the affinity of proPLA2 for the zwitterionic interface is significantly lower than it is for the anionic interface, the difference in the binding to these interfaces does not account for the >100-fold increase in activity of PLA2 over proPLA2. These results are also consistent with fluorescence anisotropy measurements with the E, E*, and E*L forms of proPLA2 (results not shown).

The interface binding environments in proPLA2 and PLA2 are different, as suggested by spectroscopic methods based mostly on the signal from Trp3. For example, as shown in Figure 2, the change in the UV absorbance spectrum associated with the apparent formation of the E*−Ca−MJ33 complex on the zwitterionic deoxy-LPC micelle interface is significantly different for the ternary complex with PLA2 and proPLA2. It should be noted that deoxy-LPC, which lacks an *sn*-2 chain, was chosen since it does not bind in the active sites of proPLA2 or PLA2, yet it can provide the interface for the binding of the enzyme with or without an occupied active site (E−Ca/E*−Ca → E*−Ca−MJ33) (*17*). The starting state of proPLA2 in these difference spectra is predominantly the E−Ca form, whereas for PLA2, the starting state is roughly 50% E−Ca and 50% E*−Ca (estimates based on the K_d values in Table 2). Regardless, in both PLA2 and proPLA2, the difference spectra qualitatively suggest that Trp3 has moved from an aqueous environment (E) to a less polar (E*) environment as suggested by the main peak in the 290 nm region. It should be noted that the change in the intensity in the difference spectrum reflects the fraction of the enzyme in the E*−MJ33 form, while the shape of the difference spectra, in particular, peaks at 288 and 292 nm, is attributed to the Trp3 environment. These difference spectra for PLA2 or proPLA2 binding MJ33 at the interface are strikingly similar to those observed by the Utrecht group (*32*, *34*) with the enzyme binding to SDS. The intensity change at 292 nm as a function

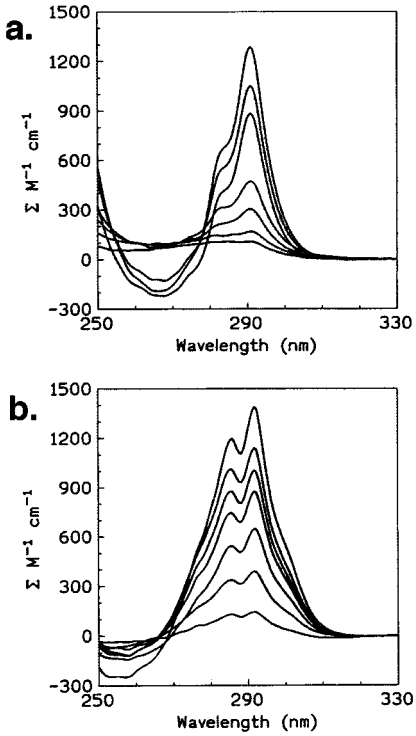

FIGURE 2: Uncorrected MJ33-induced change in the UV absorption spectrum of 0.035 mM proPLA (a) and 0.035 mM PLA2 (b) in 3 mM deoxy-LPC.

Table 3: Aggregate Size (MW in kDa) under Different Conditions[a]

additive	proPLA2	PLA2
none	13−17	13−17
DC_8PM-ether (0.3 mM)	>5000	>2000
DC_8PC-ether (0.2 mM)	15	15
DC_8PC-ether (0.2 mM) and MJ33 (0.02 mM)	>500	>100

[a] Only the lower limit estimates of the particle size are given because there are large uncertainties in the particle sizes, possibly due to the protein and amphiphile concentration dependence.

of the mole fraction of the inhibitor (*21*) suggests that the affinities of MJ33 for PLA2 and proPLA2 are not significantly different. This is also consistent with the observation that the $X_I(50)$ values (inhibitor mole fraction of half-activity) for the two enzymes are also comparable, implying that the K_M* values for the substrate are also comparable. Note that the apparent affinity for the binding of calcium in the presence of the inhibitor is considerably lower for proPLA2 (Table 2). This is probably due to the structural differences between the calcium coordination environment of PLA2 and proPLA2 (see below).

Both PLA2 and proPLA2 are known to interact with the interface of anionic amphiphiles (*31*). The solution studies with DC_8PM-ether are particularly informative because the amphiphile can both occupy the active site and provide the interface for binding (E* + Ca + DC_8PM-ether → E*−Ca−DC_8PM-ether). As summarized in Table 3, the particle size of the complexes with the ether analogues of the anionic substrate is large if the active site of the bound enzyme is occupied. Fluorescence emission intensity changes, which accompany the binding to micelles, suggest that the overall process involves at least two steps (Figure 3). As shown in Figure 3a, in the absence of calcium, the change in the emission spectrum associated with the E to E* step for the

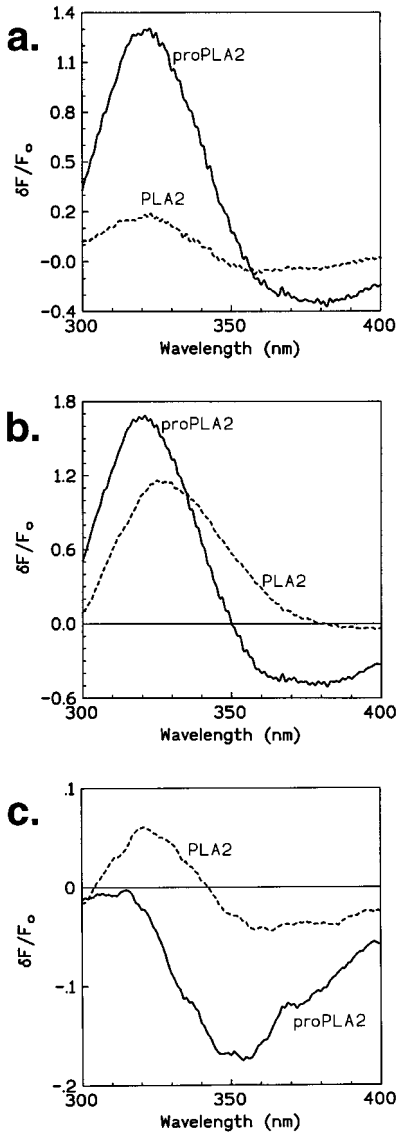

FIGURE 3: Fluorescence emission spectrum of PLA2 and proPLA2 with 0.5 mM DC_8PM-ether (a) without calcium, (b) with 0.5 mM calcium, and (c) with 0.028 mM DC_8PM-ether and calcium. For each spectrum, measurements were taken at the same concentration of PLA2 or proPLA2 on the same intensity scale without normalization. The relative δF is defined as $(F - F_0)/F_0$, where F_0 and F are the intensity without and with the DC_8PM-ether phospholipid, respectively.

binding of proPLA2 to the anionic interface is large compared to that seen with the binding of PLA2. On the other hand, as shown in Figure 3b, the spectral change in the presence of calcium, associated with the change from E−Ca to E*−Ca−DC_8PM-ether complex formation at the interface, shows an additional increase in the emission intensity that is significantly larger for PLA2 than for proPLA2. The maximum change in the emission spectra shown in these figures was obtained with micellar aggregates at a concentration of 0.5 mM DC_8PM-ether, which is twice the CMC value of 0.25 mM. Note that in both panels a and b of Figure 3 the difference spectra are shifted to the blue, suggesting Trp3 moves from an aqueous to a less polar environment. In contrast, as shown in Figure 3c, the emission signal in the presence of calcium and 0.028 mM DC_8PM-ether, which corresponds to the formation of premicellar aggregates, is significantly different for PLA2 and proPLA2. Together,

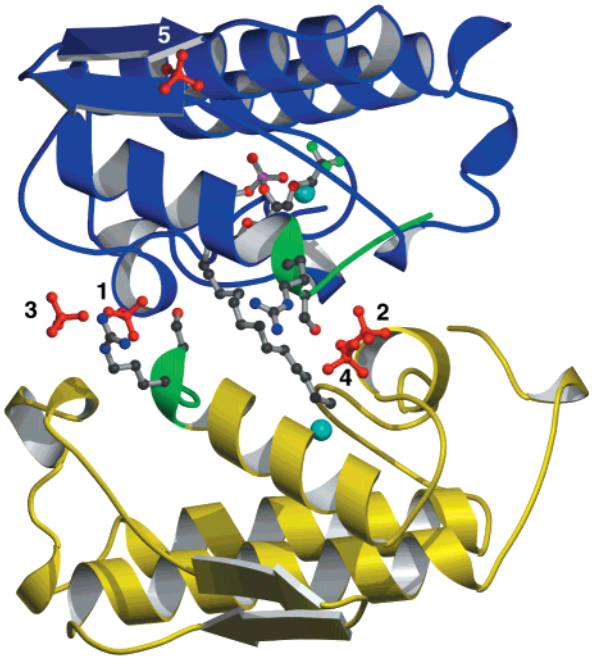

FIGURE 4: Dimer of proPLA2 with one MJ33 molecule shared between two subunits with four bound coplanar sulfate anions and a fifth sulfate near the top of subunit A (blue). The *sn*-2 phosphate of MJ33 is coordinated to the calcium ion (cyan) in subunit A, and the *sn*-1 alkyl tail extends across the subunit−subunit interface into the active site of subunit B (yellow). Four of the five sulfate anions (numbering consistent with Table 5) are coplanar and bridge the subunit−subunit interface. The propeptide of both subunits is shown in green, and Arg−1 and Ser−2, which make up part of the anion binding sites, are included in ball-and-stick form in both subunits. This figure was created using the programs MOLSCRIPT (*41*), POVSCRIPT (E. Peisach and D. Peisach), and POVRAY (http://www.povray.org).

these results suggest that the interaction of anionic amphiphiles with proPLA2, and possibly with PLA2, is a multistep process that begins to occur well below the CMC.

Crystallographic Structure of the Anion-Assisted Dimer of ProPLA2 as the i-Face Mimic. The ribbon model of the dimer contained within an asymmetric unit of proPLA2 refined to a resolution of 1.5 Å is shown in Figure 4, and a summary of the statistics of data collection and refinement is given in Table 4. The structure is composed of two subunits of the zymogen in asymmetric contact along the same surface on the protein. The ordered prosequence of each subunit, which is shown in green in Figure 4, extends the N-terminal helix of PLA2 by one turn. The dimer asymmetrically shares a single molecule of the inhibitor MJ33, and the contact is bridged by four coplanar sulfate anions. As discussed below, the overall protein conformation demonstrates significant order in regions that were disordered in previously determined structures of proPLA2 (*10*−*12*) and PLA2 (*3*−*5*). Alternate side chain conformations past C_β have been modeled in for 12 residues. Only residues 120−123 in the C-terminus of subunit B and propeptide residues Glu−6 and Gln−7 in subunit A were not clearly identified in the model due to disorder.

Anion Binding Sites. Four coplanar sulfate anions were identified at the subunit contact surface during model building. Specific anion contacts with the side chains, backbone, and bound water molecules are listed in Table 5.

Table 4: Crystal Structure Determination for the ProPLA2−MJ33 Complex

data collection	
space group	$P2_1$
cell parameters	
a (Å)	37.49
b (Å)	54.85
c (Å)	56.90
no. of subunits per asymmetric unit	2
resolution (Å)	1.45
completeness (%)	91
R_{merge}[a]	0.030
refinement	
resolution range (Å)	20.0−1.5
$R_{working}$[b]	0.21
R_{free}[b]	0.24
rmsd	
bond lengths (Å)	0.005
bond angles (deg)	1.1
total no. of non-hydrogen atoms	2359
total no. of water molecules	294

[a] $R_{merge} = \sum|I_o - I_a|/\sum(I_a)$, where I_o is the observed intensity and I_a is the average intensity, the sums being taken over all symmetry-related reflections. [b] *R*-factor $= \sum|F_o - F_c|/\sum(F_o)$, where F_o is the observed amplitude and F_c is the calculated amplitude. R_{free} is the equivalent of $R_{working}$, except it is calculated for a randomly chosen set of reflections that were omitted (10%) from the refinement process (*40*).

A fifth sulfate anion interacting with Lys87 and Asn85 in subunit A was also observed. Each modeled sulfate has a low *B*-factor and clearly interpretable electron density. Figure 5a shows a representative electron density map and ligand interactions. Propeptide residues Arg−1 and Ser−2 form part of the binding pocket for the four coplanar sulfate-binding sites at the dimer interface. Note that all the anions (Table 5) have one or two cationic ligands, while their other ligands are from the backbone amides and water molecules.

The Propeptide and 69-Loop Are Ordered. Crystal structures of proPLA2 reported previously have a disordered 69-loop (residues 61−72) and propeptide (*10*−*12*). The observation of both an ordered 69-loop and a propeptide in the proPLA2 dimer structure is likely due to hydrophobic and specific anion contacts provided by the protein−protein interface and mediating sulfate anions.

Subunit Contact Surface. There is a dramatic change in the specific anion contacts and the molecular footprint between the structure of the anion-assisted dimer of proPLA2 presented here and the corresponding PLA2 dimer structure (*15*). The propeptide of the zymogen extends into the contact region. As noted earlier, Arg−1 and Ser−2 contribute to the anion binding sites on the i-face of proPLA2, which accounts for a major difference in the anion binding sites between proPLA2 and PLA2. These interactions directly control the positioning of proPLA2 along the dimer contact surface and thereby affect several other regions. Of particular interest are the differences in the interaction of the 69-loop and C-terminus with the contact surface and therefore with the substrate interface.

These interactions are likely to be analogous to the interaction of proPLA2 with the interface of a substrate aggregate. Therefore, the structural observation of the propeptide and the accompanying other changes is relevant to understanding why the zymogen is catalytically impaired. Both the propeptide and the 69-loop make up a large portion of the protein−protein contact surface of the proPLA2 dimer.

Table 5: Coordination of Sulfate Anions in the ProPLA2 i-Face Dimer

anion	residue/atom type	subunit	distance[a] (Å)
SO_4 (1)			
O1	S−2[b], N	B	2.86
O2	R6, NE	A	2.96
	L19, N	A	2.87
O3	R6, NH2	A	2.91
	w50		2.60
O4	M20, N	A	3.12
SO_4 (2)			
O1	R6, NH2	B	2.95
	w45		2.66
O2	R6, NE	B	2.92
	L19, N	B	2.88
O3	S−2, N	A	2.87
	w31		2.78
O4	M20, N	B	3.05
SO_4 (3)			
O1	w50		2.69
O2	R−1, NH2	B	2.94
	R−1, NE	B	2.96
	R6, NH2	A	2.86
	w97		3.04
O3	K10, NZ	A	3.21
	w105		2.79
SO_4 (4)			
O1	R−1, NH2	A	4.35
	w298		2.80
O2	R−1, NH2	A	4.50
	R6, NH2	B	3.58
	w189		2.76
O3	K10, NZ	B	2.70
	w99		2.92
SO_4 (5)			
O2	K87, NZ	A	3.37
	N85, ND2	A	3.04
O3	N85, ND2	A	2.77
O4	K87, N	A	3.13
	w181		3.21

[a] Distances to the anion are listed for all protein side chains (<4.5 Å) and ordered water molecules (<3.5 Å) showing interactions with the five sulfate ions. [b] Negative sequence numbers indicate a residue is on the propeptide.

The propeptide extends the N-terminal helix one turn beyond the N-terminus of the active PLA2 and does not block the active site slot (Figure 4). Also noteworthy is the fact that the catalytically important Tyr69 is displaced from the active site and forms part of the protein−protein contact surface. The dimer proPLA2 structure indicates that close-range interactions of the anions through protein-mediated hydrogen bonds, as well as hydrophobic interactions with the interface, may be necessary for the ordering of the otherwise mobile segments.

ProPLA2 Active Site. Both subunits A and B of the proPLA2 dimer have bound calcium with an axially ligated water molecule and three backbone carbonyls from residues 28, 30, and 32 of the Ca-binding loop. The calcium in subunit B has a total of seven ligands with the addition of a bidentate carboxylate of Asp49 and another equatorial water molecule. In subunit A, the bound calcium ion is six-coordinate with the side chain of Asp49 clearly monodentate and no additional water molecule. The sixth ligand is the *pro-R* oxygen of the *sn*-2 phosphate of the MJ33 inhibitor. The two subunits share a single molecule of MJ33. The hexadecyl tail of MJ33 extends out of subunit A into the active site on the contact face with subunit B. The active site interactions in subunit A are shown in Figure 5b along with representative electron density for MJ33. A notable interaction of the tetrahedral intermediate mimic portion of MJ33 in subunit A is the hydrogen bond between His48 Nδ1 and the *pro-S* oxygen of the MJ33 inhibitor. This interaction has been observed previously for a monomeric form of PLA2 complexed with MJ33 (*35*). It is noteworthy that this monomeric PLA2 structure lacks any bound anions and may be representative of a non-interface-bound form of the enyzme. In contrast, the anion-assisted dimer structure of PLA2, which mimics the anionic interface-bound form, has an intervening water molecule between His48 Nδ1 and the *pro-S* oxygen of the MJ33 inhibitor (*15*). A schematic of <5 Å contacts made between the MJ33 inhibitor in subunit A of proPLA2 (Figure 6a) are compared with the analogous contacts of the anion-assisted PLA2 dimer structure (Figure 6b). Together, the crystallographic results show significant differences between proPLA2 and PLA2 in the subunit contact surfaces as well as the environment of the *sn*-2 tetrahedral intermediate mimic in the active site.

DISCUSSION

The spectroscopic and kinetic results in this paper show that proPLA2 binds to an anionic interface, and that the binding of the active site-directed mimics at the interface is calcium-dependent. Like PLA2 (*20*), proPLA2 shows no detectable rate of hydrolysis of monodisperse phosphatidylcholine substrates if anomalous reactions at extraneous surfaces are eliminated, such as air bubbles and vessel walls. The very low affinity of proPLA2 for the zwitterionic interface could account for an undetectable rate of hydrolysis at the phosphatidylcholine interfaces without any anionic charge. On the basis of these observations, the conflicting results and conclusions in the literature are attributed to the assay systems where the binding and the turnover steps are not adequately resolved, and the anionic charge at the interface is not adequately controlled.

ProPLA2 hydrolyzes anionic or zwitterionic substrates at the anionic interface irrespective of whether the anionic charge is induced by 4 M NaCl, the anionic additive HDS, or anionic substrates that are premicellar or larger vesicles. Compared to the rate observed with PLA2 under comparable conditions, the turnover rate of the zymogen at anionic interfaces is impaired by a factor of at least 100. Evidence at hand suggests that overall, proPLA2 has an impaired k^*_{cat} compared to that of PLA2. However, as in PLA2, anionic charges at the interface are likely responsible for an enhancement of the k^*_{cat} step of the proPLA2-catalyzed reaction. This hypothesis is consistent with a two-state model for allosteric k^*_{cat} activation (*36*) shown in Scheme 1 where the charge compensation of cationic residues 53, 56, and 120 by the negative charge on the interface converts the inert E*S complex to a catalytically active complex $(E^*S)^\#$ of PLA2 as modeled in Scheme 1. According to this model, the lower k^*_{cat} observed for proPLA2 results from a compromised ability to form the active $(E^*S)^\#$ form (*33*, *37*). Results in this paper are also consistent with an alternate explanation, where only a small fraction of proPLA2 at the anionic interface is present in the activated form.

Relationship of the Anion Binding Sites to Interface Binding. The results obtained with the enzyme in aqueous phospholipid dispersions correlate with the crystal structure

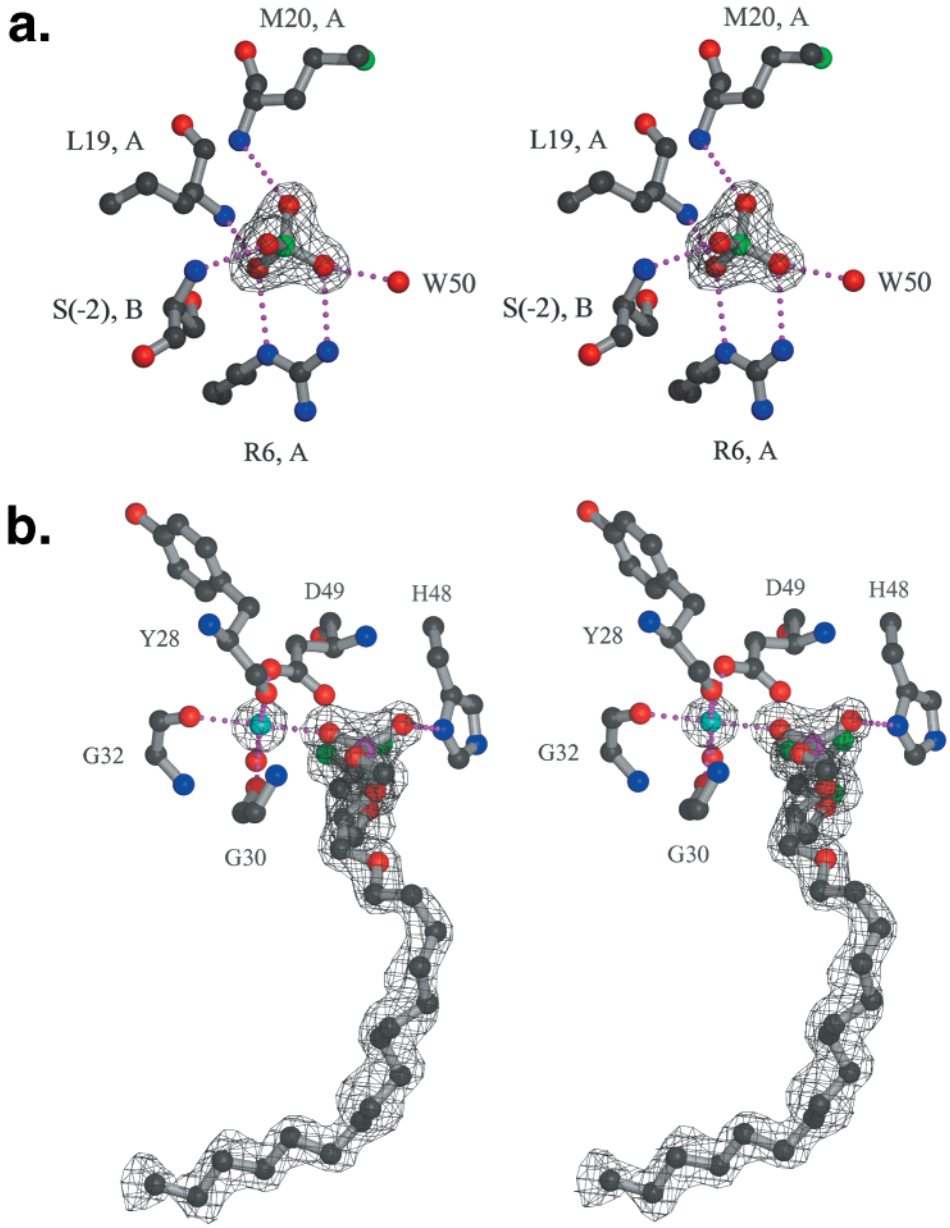

FIGURE 5: Representative electron density maps ($2F_o - F_c$ coefficients) are shown as stereoviews. (a) Bound sulfate anion 1 from Table 5 is ligated by Arg6, Leu19, and Met20 from subunit A along with Ser−2 from subunit B and water 50 (w50). (b) The active site of subunit A is displayed, including the final electron density ($2F_o - F_c$) of the calcium and the MJ33 inhibitor. The calcium is coordinated to the backbone carbonyls of Tyr28, Gly30, and Gly32 of the Ca-binding loop, bidentate by Asp49, the *pro-R* oxygen of the *sn*-2 phosphate of the MJ33 inhibitor, and an axial water, w12. The catalytically important His48 is also shown H-bonded to the *pro-S* oxygen of MJ33. This figure was created using the programs MOLSCRIPT (*41*), POVSCRIPT (E. Peisach and D. Peisach), and POVRAY (http://www.povray.org).

of the anion-assisted dimer of proPLA2 with MJ33 in the catalytic site. As discussed below, an understanding of how the propeptide compromises the catalytic efficiency is provided by clear differences in how PLA2 versus proPLA2 would interact with the interface, and as a result how their active sites and mechanistic intermediates differ. The comparison of the structures of the proPLA2 and PLA2 (*15*) dimer provides insight into the putative i-face of PLA2 (Figure 7). The i-face mimic forms of proPLA2 and PLA2 that will be discussed are obtained by removing the subunit from each dimer that binds the *sn*-1 alkyl tail of the inhibitor MJ33. This leaves a model for each that includes a single subunit complexed to the *sn*-2 phosphate of the tetrahedral mimic MJ33 and coplanar anions, as depicted in panels b and c of Figure 7. These models are consistent with the consensus mechanism of PLA2 catalysis in which a single subunit of PLA2 is bound to the interface (*38*). As an interface-bound mimic, the subunit−subunit contact in the anion-assisted dimer of PLA2 with five coplanar anions (Figure 7e) is different from that in the dimer of proPLA2 with four anions (Figure 7d). Also, the hydrophobic contact region in the dimer of proPLA2 is noticeably altered from that for PLA2. Since the anions bring the hydrophobic and hydrogen-bonding groups of the enzyme's i-face in close contact in the dimer seen in these crystal structures, a comparable relationship is likely between a single subunit of proPLA2 or PLA2 during the high-affinity contact along the i-face with the anionic groups at the substrate interface during the interfacial processive turnover. These models are consistent with the fluoresence emission spectroscopy results

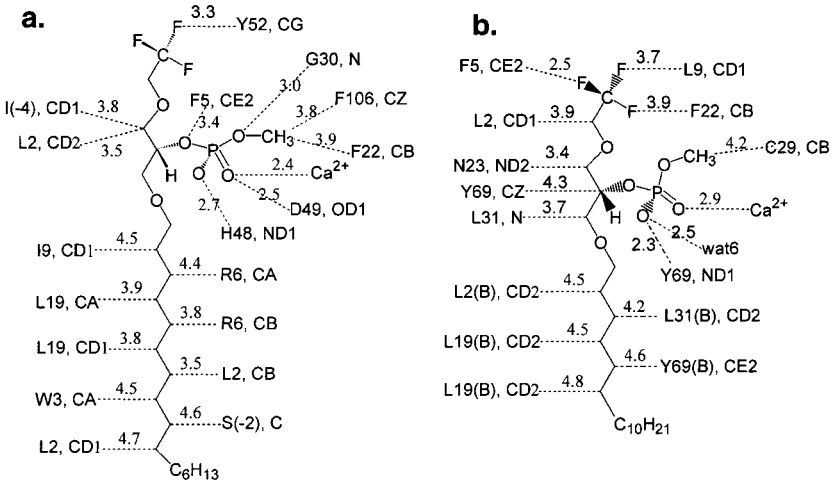

FIGURE 6: Schematic of the MJ33 inhibitor with major contacts made within the A subunits shown as dashed lines for the (a) proPLA2 i-face-bound mimic structure and (b) the PLA2 i-face-bound mimic structure (*15*). Several interactions of MJ33 with subunit B are denoted by a B next to the residue.

that confirm that proPLA2 and PLA2 have altered modes of binding to an anionic interface. Other significant structural features of PLA2 and proPLA2 are compared below. While it remains to be established whether such structural differences constitute the primary basis for the functional difference between PLA2 and proPLA2, as developed later w6, a water molecule in the outer coordination sphere of calcium, seen in PLA2 but not in proPLA2, is mechanistically implicated.

Propeptide and 69-Loop Movement. The previously observed disorder of the propeptide (*10*−*12*) was suggested as a reason proPLA2 is inactive (*31*). The disordered propeptide could propagate the disorder of the N-terminus of the enzyme, thereby disrupting a critical hydrogen bond network involving the free NH_2 group of Ala1 (*3*). The propeptide is ordered in the current zymogen structure. The overlay of PLA2 and proPLA2 in Figure 7a shows how the ordered propeptide extension of the N-terminal α-helix in proPLA2 clashes with the position of the 69-loop from the active form PLA2 structure. This suggests one of the possible functions for the propeptide is to alter the conformation of the mechanistically significant 69-loop.

In general, several loops of the anion-assisted dimer structures are more ordered than the other PLA2 structures. This suggests that the catalytically relevant interface-bound structure may be more ordered. The proPLA2 anion binding observed by Arg−1 and Ser−2 suggests a more direct role for the propeptide in positioning proPLA2 on an anionic interface. In the dimer of PLA2 (*15*), the two helices (residues 39−57 and 89−108) appear to be parallel to the interface; however, this is not the case in the zymogen stucture shown in Figure 7b, where these two helices display a noticeable tilt relative to the plane defined by the four coplanar anion binding sites and the dimer interface. Following the cleavage of the propeptide to form active PLA2, the enzyme adopts a noticeably different orientation relative to the coplanar anions and by inference the interface as shown in Figure 7c. The difference spectra of Trp3 in the E*−MJ33 form (Figure 2) also support an altered interface for proPLA2 and active PLA2. In addition to a change in anion binding sites between the pro and active enzyme, the footprint of interface binding varies dramatically as suggested by the comparison of the desolvated dimer interface for proPLA2 (Figure 7d) and PLA2 (Figure 7e). Here a significantly altered position of the 69-loop (Figure 7a) caused by the propeptide also modifies the interface contact of proPLA2 relative to the active enzyme.

We propose that a coupling between interface contacts of the 69-loop and the resulting side chain conformers of Tyr-69 gives rise to the activated and less active forms of the enzyme. Tyr69 is proposed to regulate k^*_{cat} on an anionic interface (*7*) by stabilizing the E*S complex or by stabilizing the negative charge on the product that could facilitate the collapse of the tetrahedral intermediate (*18*, *35*). The location of the 69-loop controls the positioning of the hydroxyl of Tyr69, which has been shown to interact with the *pro-S* oxygen of the *sn*-2 phosphate of the tetrahedral intermediate mimic in the anion-assisted dimer of PLA2 (*15*). However, the effect of the Tyr69 → Phe mutation on catalysis is modest with a mere 10-fold reduction in k^*_{cat} (*7*). At this point, it is unclear what the precise functions of the 69-loop and residue Tyr69 are, but it is apparent that the repositioning of the 69-loop in proPLA2 has a dramatic effect on how the enzyme sits on the interface.

Interface Binding Affects Inhibitor Binding. The change in interface binding between proPLA2 and PLA2 is accompanied by an altered mode of MJ33 inhibitor binding to the active site. The differential binding of MJ33 to proPLA2 versus PLA2 suggests an impaired conformation of the enzyme−tetrahedral intermediate species of the zymogen. The *sn*-3 chain of the proPLA2−MJ33 dimer is bound into a hydrophobic pocket formed by the propeptide and the helix of residues 40−57. In contrast, the PLA2−MJ33 dimer structure (*15*) cannot form this hydrophobic pocket due to the absence of the propeptide. The dramatically changed position of the 69-loop in PLA2 (Figure 7a) creates a new hydrophobic pocket that does not exist in PLA2 between the 69-loop and the N-terminal helix. The alternate modes for binding of the substrate to PLA2 versus proPLA2 may distinguish the catalytically active form of the substrate.

Calcium-Coordinated Activated Water Mechanism. Active site waters play a crucial role in the calcium-coordinated oxyanion mechanism (Scheme 2). In fact, evidence developed below suggests that the presence or absence of a single

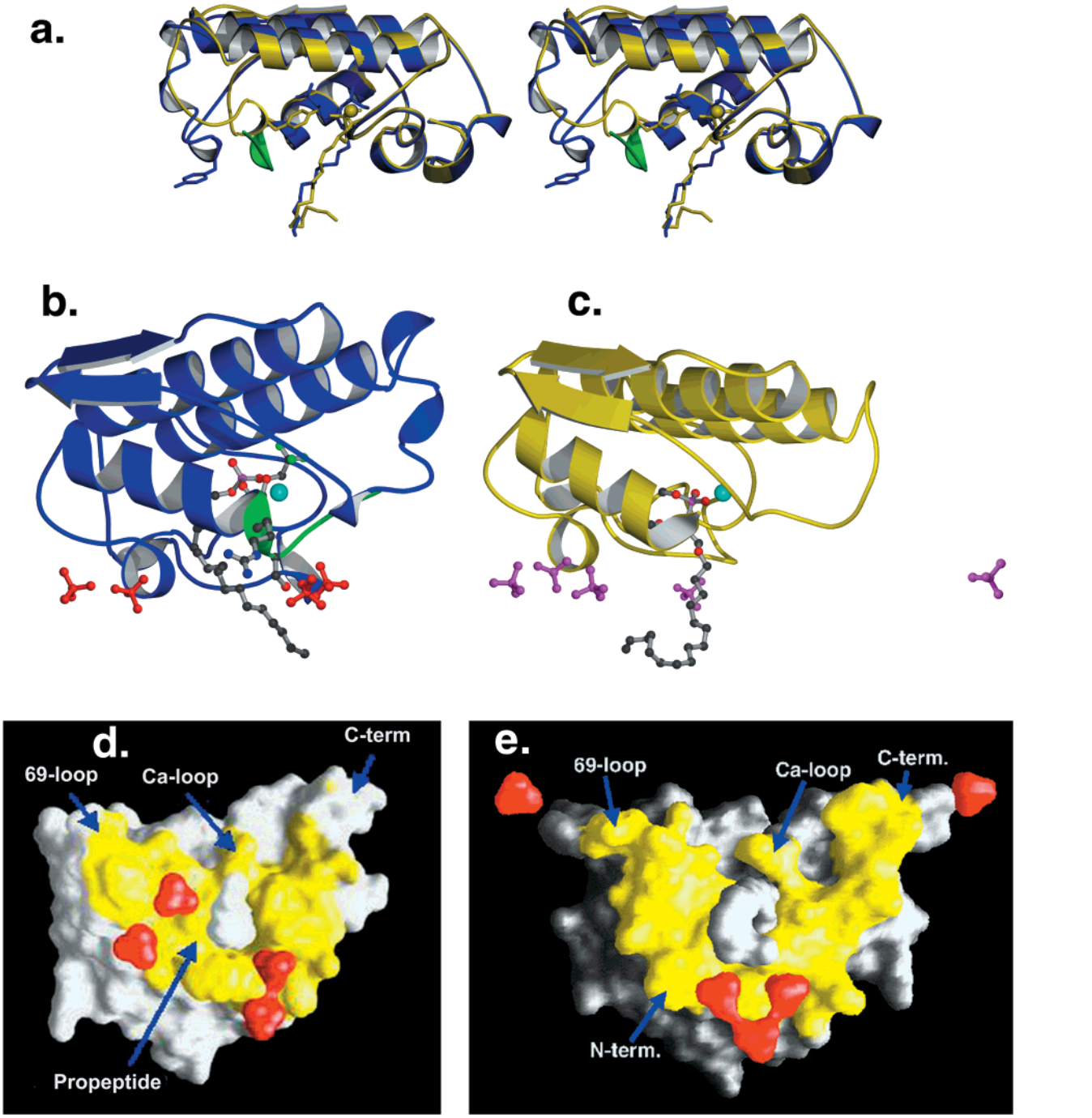

FIGURE 7: Comparison of the i-face binding surfaces of proPLA2 and PLA2 from the anion-assisted dimer structures. (a) Stereoview overlay of subunit A of the current dimer proPLA2−MJ33 structure (blue) and the analogous subunit from the dimer PLA2−MJ33 structure (yellow) (*15*). The propeptide of the proPLA2 structure is shown in green. Tyr69 on the 69-loop is clearly visible from each structure along with the MJ33 inhibitor. (b) Subunit A of proPLA2 (blue) with four coplanar sulfate anions, MJ33, Ca, and propeptide (green). Anion binding residues Arg−1 and Ser−2 of the propeptide are shown in ball-and-stick form. (c) Subunit A of the anion-assisted dimer structure of the PLA2−MJ33 complex relative to the five coplanar phosphate anions bound in the structure (*15*). The molecule is oriented like the proPLA2 depicted in panel b with the anions defining a plane on the horizontal. Note the orientation of the top two helices and β-sheets between the proPLA2 (b) and PLA2 (c) enzymes. Panels a−c were created using the programs MOLSCRIPT (*41*), POVSCRIPT (E. Peisach and D. Peisach), and POVRAY (http://www.povray.org). (d) Interface footprint of subunit A of the current proPLA2 structure displayed as a van der Waals surface using the program GRASP (*42*). The dimer contact surface is shown orthogonal to the plane of the four coplanar sulfate anions (red) and the alkyl tail of the MJ33 inhibitor (gray) pointing outward. The solvent inaccessible dimer interface (yellow) surface area of 1449 Å^2 was calculated with a probe radius of 1.4 Å (*43*). (e) The analogous interface footprint of subunit A from the active enzyme PLA2−MJ33 structure (*15*) has a solvent inaccessible dimer interface of 1470 Å^2 (yellow). The five coplanar phosphate anions are shown in red.

critical water could correspond to the difference between the activated or inactivated form of the enzyme. Two water molecules, w5 and w6, are found in the structure of Ca-PLA2 without a mimic bound in the active site. Either the calcium-coordinated w5 (in the water-assisted oxyanion mechanism) or the w6 hydrogen bonded to catalytic H48 (in the single-water general base mechanism) could act as the nucleophile. While there is convincing kinetic evidence

Scheme 2

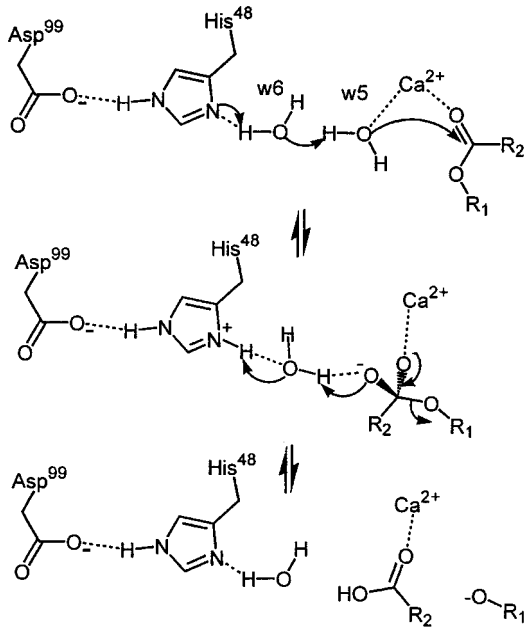

in support of the oxyanion mechanism (*7*), the second assisting water, w6, present in the outer coordination sphere of calcium, has generally not been observed in any of the structures of the PLA2−inhibitor complexes except in the structure of the anion-assisted dimer, which we believe mimics the active form at the anionic interface as discussed below.

Typically, His48 Nδ1 has been observed directly H-bonding to the inhibitor in previously determined crystal structures of active PLA2 (*35*, *39*). This is the case for the zymogen structure reported here as shown in Figure 8a. This direct interaction is also notably the case for the monomer PLA2−MJ33 structure (PDB entry 1FDK), which has the critical 69-loop and inhibitor oriented in a conformation that was suggestive of being an active conformation. However, as is the case with the proPLA2 structure, the assisting water bridging His48 and the tetrahedral intermediate mimic is not present as shown in Figure 8b (*35*). Therefore, the proPLA2 and monomeric PLA2 structures may represent a tetrahedral intermediate formed following the less activated form E*S (Scheme 1) or a dead-end complex off of the E*S form.

The only instance where the assisting water has been observed is in the previously reported active "i-face mimic" dimer structure (*15*), where a water molecule (w6) bridges His48 Nδ1 and the *pro-S* oxygen of the MJ33 inhibitor (Figure 8c). In this structure with MJ33 (Figure 8c), the *pro-S* oxygen of the *sn*-2 phosphate represents the attacking nucleophilic water labeled w5 in Scheme 2. The existence of a bridging water in the mechanism shown in Scheme 2 contrasts with a mechanism that operates with a single catalytic water poised between His48 and the substrate. It is conceivable that interfacial binding and anionic charge compensation for k^*_{cat} activation could cause the structural changes that allow the assisting water to be suitably positioned in the $(E^*S)^{\#}$ complex (Scheme 1).

To recapitulate, results in this paper suggest that the absence of w6 (Scheme 2) in proPLA2 impairs k^*_{cat}. Remarkably, this bridging water is found only in the structure of the anion-assisted dimer form of PLA2 (*15*). In the

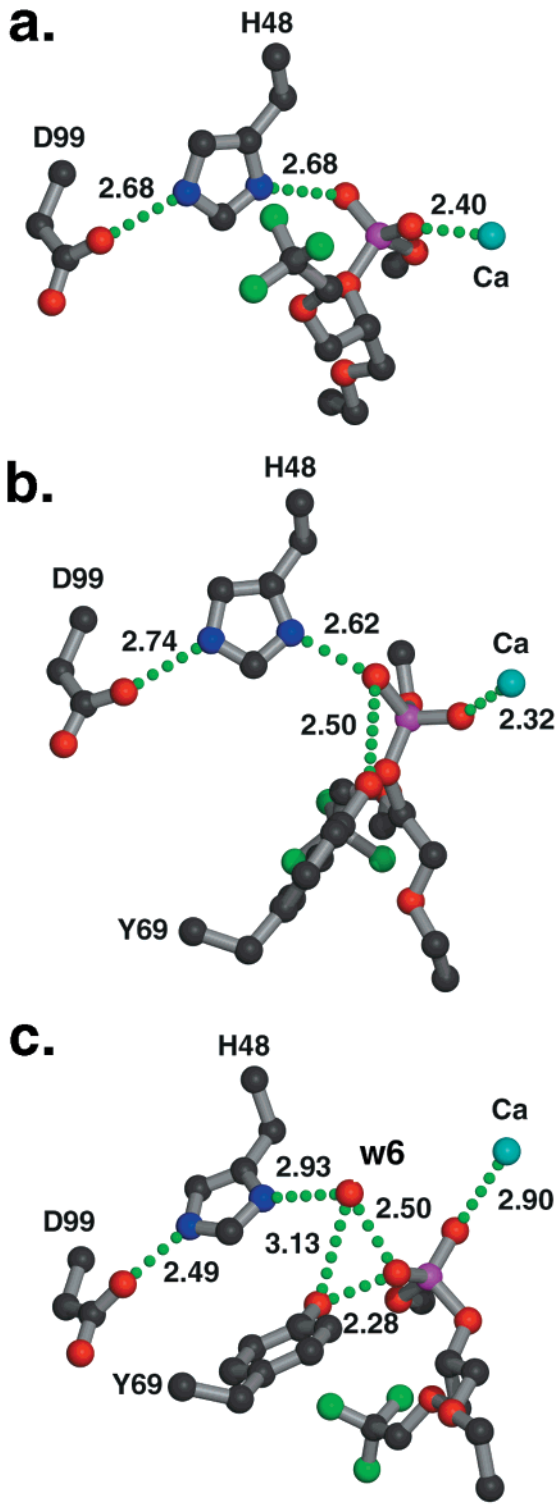

FIGURE 8: Catalytic site environment of PLA2−MJ33 complexes. H-Bonds are shown in dashed green lines with distances in angstroms. (a) Key interactions at the active site of the current proPLA2−MJ33 complex. (b) Similar view of the previously reported monomer PLA2−MJ33 complex (*35*). Tyr69 can be seen H-bonding to the *pro-S* oxygen of the *sn*-2 phosphate of the MJ33 inhibitor. (c) Similar view of the previously reported anion-assisted dimer PLA2−MJ33 structure (*15*). The assisting water w6, from the calcium-coordinated oxyanion mechanism (Scheme 2), can be seen bridging His48 and the *pro-S* oxygen of the *sn*-2 phosphate of the MJ33 inhibitor, while Tyr69 is shown H-bonding to the same *pro-S* oxygen of the inhibitor. This figure was created using the programs MOLSCRIPT (*41*), POVSCRIPT (E. Peisach and D. Peisach), and POVRAY (http://www.povray.org).

absence of w6, the chemical step may proceed with a less efficient single-water mechanism. An alternate explanation is that the structure of the proPLA2−MJ33 complex represents a dead-end species, thereby explaining the zymogen's loss of activity as a partitioning of the enzyme to an inactive form. Regardless, the mechanistic implication of the loss of activity in the zymogen suggests a critical role in the chemical step for assisting water w6 for the activated enzyme. It is not unreasonable to consider the possibility that w6, which is also a second-sphere Ca ligand and simultaneously hydrogen bonded to H48, modulates the pK_a of the catalytic water directly coordinated to calcium in the $(E^*S)^{\#}$ complex and subsequently stabilizes the tetrahedral intermediate for the rate-limiting transition state to form products.

REFERENCES

1. Jain, M. K., Gelb, M. H., Rogers, J., and Berg, O. G. (1995) *Methods Enzymol. 249*, 567−614.
2. Berg, O. G., Yu, B. Z., Rogers, J., and Jain, M. K. (1991) *Biochemistry 30*, 7283−7297.
3. Dijkstra, B. W., Kalk, K. H., Hol, W. G., and Drenth, J. (1981) *J. Mol. Biol. 147*, 97−123.
4. Scott, D. L., and Sigler, P. B. (1994) *Adv. Protein Chem. 45*, 53−88.
5. Steiner, R. A., Rozeboom, H. J., de Vries, A., Kalk, K. H., Murshudov, G. N., Wilson, K. S., and Dijkstra, B. W. (2001) *Acta Crystallogr. D57*, 516−526.
6. Verheij, H. M., Slotboom, A. J., and de Haas, G. H. (1981) *Rev. Physiol. Biochem. Pharmacol. 91*, 91−203.
7. Yu, B. Z., Rogers, J., Nicol, G. R., Theopold, K. H., Seshadri, K., Vishweshwara, S., and Jain, M. K. (1998) *Biochemistry 37*, 12576−12587.
8. Pieterson, W. A., Vidal, J. C., Volwerk, J. J., and de Haas, G. H. (1974) *Biochemistry 13*, 1455−1460.
9. Jain, M. K., Rogers, J., and DeHaas, G. H. (1988) *Biochim. Biophys. Acta 940*, 51−62.
10. Tomoo, K., Yamane, A., Ishida, T., Fujii, S., Ikeda, K., Iwama, S., Katsumura, S., Sumiya, S., Miyagawa, H., and Kitamura, K. (1997) *Biochim. Biophys. Acta 1340*, 178−186.
11. Finzel, B. C., Weber, P. C., Ohlendorf, D. H., and Salemme, F. R. (1991) *Acta Crystallogr. B47*, 814−816.
12. Dijkstra, B. W., van Nes, G. J. H., Kalk, K. H., Brandenburg, N. P., Hol, W. G. J., and Drenth, J. (1982) *Acta Crystallogr. B38*, 793−799.
13. Yuan, C., and Tsai, M. (1999) *Biochim. Biophys. Acta 1441*, 215−222.
14. Yu, B. Z., Rogers, J., Tsai, M. D., Pidgeon, C., and Jain, M. K. (1999) *Biochemistry 38*, 4875−4884.
15. Pan, Y. H., Epstein, T. M., Jain, M. K., and Bahnson, B. J. (2001) *Biochemistry 40*, 609−617.
16. Ramirez, F., and Jain, M. K. (1991) *Proteins: Struct., Funct., Genet. 9*, 229−239.
17. Yu, B. Z., Berg, O. G., and Jain, M. K. (1993) *Biochemistry 32*, 6485−6492.
18. Rogers, J., Yu, B. Z., Serves, S. V., Tsivgoulis, G. M., Sotiropoulos, D. N., Ioannou, P. V., and Jain, M. K. (1996) *Biochemistry 35*, 9375−9384.
19. Jain, M. K., Yu, B. Z., Rogers, J., Ranadive, G. N., and Berg, O. G. (1991) *Biochemistry 30*, 7306−7317.
20. Yu, B. Z., Berg, O. G., and Jain, M. K. (1999) *Biochemistry 38*, 10449−10456.
21. Jain, M. K., and Maliwal, B. P. (1993) *Biochemistry 32*, 11838−11846.
22. Koehler, K. A., Jain, M. K., Gabriel, D. A., Chang, H. Y., and Malhotra, O. P. (1995) *J. Protein Chem. 14*, 537−548.
23. Jain, M. K., Tao, W. J., Rogers, J., Arenson, C., Eibl, H., and Yu, B. Z. (1991) *Biochemistry 30*, 10256−10268.
24. Otwinowski, Z., and Minor, W. (1997) *Methods Enzymol. 276*, 307−326.
25. Brunger, A. T., Adams, P. D., Clore, G. M., DeLano, W. L., Gros, P., Grosse-Kunstleve, R. W., Jiang, J.-S., Kuszewski, J., Nilges, N., Pannu, N. S., Read, R. J., Rice, L. M., Simonson, T., and Warren, G. L. (1998) *Acta Crystallogr. D54*, 905−921.
26. Dijkstra, B. W., Renetseder, R., Kalk, K. H., Hol, W. G., and Drenth, J. (1983) *J. Mol. Biol. 168*.
27. Brunger, A. T., Adams, P. D., Clore, G. M., Delano, W. L., Gros, P., Grosse-Kunstleve, R. W., Jiang, J.-S., Kuszewski, J., Nilges, N., Pannu, N. S., Read, R. J., Rice, L. M., Simonson, T., and Warren, G. L. (1998) *Acta Crystallogr. D54*, 905−921.
28. Bailey, S. (1994) *Acta Crystallogr. D50*.
29. Sheldrick, G. M. (1998) in *Direct Methods for Solving Macromolecular Structures* (Fortier, S., Ed.) pp 401−411, Kluwer Academic Publishers, Dordrecht, The Netherlands.
30. Pieterson, W. A., Volwerk, J. J., and de Haas, G. H. (1974) *Biochemistry 13*, 1439−1445.
31. Volwerk, J. J., and de Haas, G. H. (1982) Vol. 1, John Wiley & Sons, New York.
32. Volwerk, J. J., Jost, P. C., de Haas, G. H., and Griffith, O. H. (1984) *Chem. Phys. Lipids 36*, 101−110.
33. Berg, O. G., Rogers, J., Yu, B. Z., Yao, J., Romsted, L. S., and Jain, M. K. (1997) *Biochemistry 36*, 14512−14530.
34. Hille, J. D., Egmond, M. R., Dijkman, R., van Oort, M. G., Sauve, P., and de Haas, G. H. (1983) *Biochemistry 22*, 5353−5358.
35. Sekar, K., Eswaramoorthy, S., Jain, M. K., and Sundaralingam, M. (1997) *Biochemistry 36*, 14186−14191.
36. Yu, B. Z., Janssen, M. J., Verheij, H. M., and Jain, M. K. (2000) *Biochemistry 39*, 5702−5711.
37. Rogers, J., Yu, B. Z., Tsai, M. D., Berg, O. G., and Jain, M. K. (1998) *Biochemistry 37*, 9549−9556.
38. Jain, M. K., Ranadive, G., Yu, B. Z., and Verheij, H. M. (1991) *Biochemistry 30*, 7330−7340.
39. Thunnissen, M. M. G. M., Ab, E., Kalk, K. H., Drenth, J., Dijkstra, B. W., Kuipers, O. P., Dijkman, R., de Haas, G. H., and Verheij, H. M. (1990) *Nature 347*, 689−691.
40. Brunger, A. T. (1992) *Nature 355*, 472−474.
41. Kraulis, P. J. (1991) *J. Appl. Crystallogr. 24*, 946−950.
42. Honig, B., and Nicholls, A. (1995) *Science 268*, 1144−1149.
43. Lee, B., and Richards, F. M. (1971) *J. Mol. Biol. 55*, 379−400.

BI011228H